

Supplementary Methods and Results
Empowering the crowd: Feasible strategies
to minimize the spread of COVID-19
in informal settlements

Alberto Pascual-García^{(1,*),} Jordan Klein⁽²⁾, Jennifer Villers^(3,^),
Eduard Campillo-Funollet^(4,^), Chamsy Sarkis⁽⁵⁾

January 21, 2021

(1) Institute of Integrative Biology. ETH-Zürich. Zürich, Switzerland.

(2) Office of Population Research. Princeton University. Princeton, NJ, USA.

(3) Princeton Environmental Institute. Princeton University. Princeton, NJ, USA.

(4) Genome Damage and Stability Centre. University of Sussex. Brighton, United Kingdom.

(5) Pax Syriana Foundation. Valetta, Malta.

(^) Equal contribution.

(*) correspondence: alberto.pascual@env.ethz.ch

Parameterization of the model

Derivation of fixed parameters (Main Table ??)

To estimate the latent period ($1/\delta_E$), we calculated the difference between randomly generated incubation ($1/\delta_E + 1/\delta_P$) and presymptomatic ($1/\delta_P$) periods. We estimated the presymptomatic period using results reported by He et al. [1] and found they best fit a Gompertz distribution with a mean of 2.3 days (95% CI: 0.8-3.0). Since a correction of these by Ashcroft et al. [2] suggests they significantly underestimate the presymptomatic period's upper bound, we estimated that the true presymptomatic period follows a Gaussian distribution around the mean (95% CI: 0.8-3.8). However, this presymptomatic period distribution implies a non-negligible probability of a negative latent period. To correct this discrepancy, we assumed a minimum latent period of .5 days [3]. Time from symptom onset to death in critical cases ($1/\alpha$) is estimated using time from symptom onset to ICU admission in Wang et al [4].

Derivation of transmissibility parameters (Main Table ??)

ρ_{HI} calculated manually from van Kampen et al.[5] by ratio of viral culture positive test rate in hospitalized patients 7-16 days since start of symptoms to positive test rate in patients 0-6 days since start of symptoms.

$$\beta_A = \beta_I \rho_{AI} \quad (1)$$

$$\beta_H = \beta_I \rho_{HI} \quad (2)$$

$$\frac{AUC_P}{(1 - AUC_P)} = \frac{\frac{\beta_P}{\delta_P}}{\frac{\beta_I}{\gamma_I} + \frac{\beta_H}{\gamma_H}} \quad (3)$$

$$\beta_I \gamma_H + \beta_H \gamma_I = \frac{\beta_P \gamma_I \gamma_H (1 - AUC_P)}{AUC_P \delta_P} \quad (4)$$

$$\beta_I \gamma_H + \beta_I \rho_{HI} \gamma_I = \frac{\beta_P \gamma_I \gamma_H (1 - AUC_P)}{AUC_P \delta_P} \quad (5)$$

$$\beta_I = \frac{\beta_P \gamma_I \gamma_H (1 - AUC_P)}{AUC_P \delta_P (\gamma_H + \rho_{HI} \gamma_I)} \quad (6)$$

$$\beta_A = \frac{\rho_{AI} \beta_P \gamma_I \gamma_H (1 - AUC_P)}{AUC_P \delta_P (\gamma_H + \rho_{HI} \gamma_I)} \quad (7)$$

$$\beta_H = \frac{\rho_{HI} \beta_P \gamma_I \gamma_H (1 - AUC_P)}{AUC_P \delta_P (\gamma_H + \rho_{HI} \gamma_I)} \quad (8)$$

Population structure of demographic-classes derivation (Main Table ??)

In April, 2020, 40.7% of the population in informal IDP camps in Northern Syria was aged 0-12, 53.4% aged 13-50, and 5.9% aged 51+ [6]. We assumed the age-specific prevalence of chronic disease is comparable in Syrian refugees in both Syria and Jordan. According to survey data on Syrian refugees in Jordan, 10% of people under 30, 30% of people 30-50, and 50% of people over 50 reported having chronic diseases [7]. We assumed that no one in the 0-12 age group had chronic diseases and calculated the proportion of people aged 13-50 with chronic diseases by standardizing the age-specific chronic disease prevalence reported in the survey to the age distribution in the 13-50 interval of the IDP camp population. In sum, we assume that ~17.7% of adults aged 13-50 and 50% of adults aged 51+ have comorbidities.

Epidemiological severity derivation

We estimated the fractions of symptomatic cases in children aged <13 that would become severe and critical from the fractions of symptomatic cases in children aged <11 that were severe and critical in China [8]. We estimated the class-specific fractions of symptomatic cases in adults that would become severe and critical using the age and comorbidity-specific fractions of symptomatic cases with known outcomes that required hospitalization, without and with ICU admission, respectively in the United States [9]. To account for poorer health among Syrian adults compared to their similarly aged peers in developed countries, estimates for US adults aged 19-64 were used for Syrian adults aged 13-50, while estimates for US adults aged 65+ were used for Syrian adults aged 51+.

Derivation of the transmissivity parameter τ

Estimation of the Next Generation Matrix

In the following, to simplify the notation we define $\kappa_i = ((1 - g_i - h_i)\gamma_I + h_i\eta + g_i\alpha)$. To estimate the probability of infection if there is a contact between a susceptible and an infected individual (parameter τ) we proceed as follows [10, 11, 12]. We start by considering the subsystem containing the infected population:

$$\dot{E}_i = \lambda_i S_i - \delta_E E_i \quad (9)$$

$$\dot{P}_i = \delta_E E_i - \delta_P P_i \quad (10)$$

$$\dot{A}_i = (1 - f)\delta_P P_i - \gamma_A A_i \quad (11)$$

$$\dot{I}_i = f\delta_P P_i - \kappa_i I_i \quad (12)$$

$$\dot{H}_i = h_i\eta I_i - \gamma_H H_i. \quad (13)$$

For the sake of simplifying the notation, let us consider the following ordering of the variables in the vector $x = (E_1, \dots, E_M, P_1, \dots, P_M, A_1, \dots, A_M, I_1, \dots, I_M, H_1, \dots, H_M)$, with M the number of population classes. We are interested in the parameterization of the null model, which will serve as a baseline to estimate the parameter τ , which is initially unknown, but does not change when interventions are introduced. Considering the contacts matrix for the null model (Eq. ?? in Main Text), the rate of exposure becomes

$$\lambda_i = \frac{\tau}{N} \sum_{j=1}^n \bar{c}_i^0 (\beta_P P_j + \beta_A A_j + \beta_I I_j + \beta_H H_j).$$

In the following, we use bold symbols for vectors and matrices, and the symbols \odot and \oslash for the element-wise product and division, respectively. Following this notation, the linearized system can be written in the form $\dot{x} = (\mathbf{T} + \Sigma)x$, where:

$$\mathbf{T} = \tau \begin{bmatrix} 0 & \Theta & \Theta & \Theta & \Theta \\ 0 & 0 & 0 & 0 & 0 \\ 0 & 0 & 0 & 0 & 0 \\ 0 & 0 & 0 & 0 & 0 \\ 0 & 0 & 0 & 0 & 0 \end{bmatrix} \quad (14)$$

is the transmission matrix, with $\Theta = \text{diag}(\mathbf{p} \odot \bar{\mathbf{c}}^0) \mathbf{U}$, $\{\mathbf{p}\} = N/N$, and \mathbf{U} is the all ones matrix of size M . The transition matrix is

$$\Sigma = \begin{bmatrix} -\delta_E \mathbf{I} & \mathbf{0} & \mathbf{0} & \mathbf{0} & \mathbf{0} \\ \delta_E \mathbf{I} & -\delta_P \mathbf{I} & \mathbf{0} & \mathbf{0} & \mathbf{0} \\ \mathbf{0} & (1-f)\delta_P \mathbf{I} & -\gamma_A \mathbf{I} & \mathbf{0} & \mathbf{0} \\ \mathbf{0} & f\delta_P \mathbf{I} & \mathbf{0} & -\text{diag}(\boldsymbol{\kappa}) \mathbf{I} & \mathbf{0} \\ \mathbf{0} & \mathbf{0} & \mathbf{0} & \eta \text{diag}(\mathbf{h}) \mathbf{I} & -\gamma_H \mathbf{I} \end{bmatrix} \quad (15)$$

Where \mathbf{I} and $\mathbf{0}$ are the identity and null matrices of size M , and $\boldsymbol{\kappa} = \mathbf{l}\gamma_I + \mathbf{h}\eta + \mathbf{g}\alpha$. We next compute the inverse of the transition matrix

$$\Sigma^{-1} = \begin{bmatrix} -\frac{1}{\delta_E} \mathbf{I} & \mathbf{0} & \mathbf{0} & \mathbf{0} & \mathbf{0} \\ -\frac{1}{\delta_P} \mathbf{I} & -\frac{1}{\delta_P} \mathbf{I} & \mathbf{0} & \mathbf{0} & \mathbf{0} \\ -\frac{(1-f)}{\gamma_A} \mathbf{I} & -\frac{(1-f)}{\gamma_A} \mathbf{I} & -\frac{1}{\gamma_A} \mathbf{I} & \mathbf{0} & \mathbf{0} \\ -f \text{diag}(\boldsymbol{\kappa}^{-1}) \mathbf{I} & -f \text{diag}(\boldsymbol{\kappa}^{-1}) \mathbf{I} & \mathbf{0} & -\text{diag}(\boldsymbol{\kappa}^{-1}) \mathbf{I} & \mathbf{0} \\ -\frac{f\eta}{\gamma_H} \text{diag}(\mathbf{h} \otimes \boldsymbol{\kappa}) \mathbf{I} & -\frac{f\eta}{\gamma_H} \text{diag}(\mathbf{h} \otimes \boldsymbol{\kappa}) \mathbf{I} & \mathbf{0} & -\frac{\eta}{\gamma_H} \text{diag}(\mathbf{h} \otimes \boldsymbol{\kappa}) \mathbf{I} & -\frac{1}{\gamma_H} \mathbf{I} \end{bmatrix} \quad (16)$$

The NGM with large domain can now be found by $\mathbf{K}_L = -T\Sigma^{-1}$. However, since we know that each individual who gets infected becomes exposed (E compartment), we focus on the NGM with small domain, \mathbf{K}_S , which only consists of the E compartment [13]. We do this by removing the rows that correspond to the other compartments from T and the columns from Σ^{-1} . We then find:

$$\mathbf{K}_S = \tau \left[\left(\frac{1}{\delta_P} + \frac{(1-f)}{\gamma_A} \right) \Theta + \text{diag} \left(f \mathbf{h}^{-1} \left(1 + \frac{\eta}{\gamma_H} \mathbf{h} \right) \right) \Theta \right].$$

The reproduction number is related to the main eigenvalue of \mathbf{K}_S , i.e. $R_0 = |\lambda_1|$, and τ is estimated from the main eigenvalue of $\tilde{K}_S = K_S/\tau$. Considering the null model parameters $(\tilde{\lambda}_1^0)$, we have the expression:

$$\tau = \frac{R_0}{|\tilde{\lambda}_1^0|}. \quad (17)$$

Parameterization of the interventions

Safety zone

We considered the existence of a safety zone to protect a certain fraction, f_S , of the population, mostly those more vulnerable. In practice, this involves dividing the camp in two areas, a “green” zone (denoted g) for the protected population and an “orange” zone (o) for the exposed population. These two populations could interact via a buffer zone, under controlled conditions. Based on our assumption that infectivity in the buffer zone is reduced by 80%, $\hat{\tau} = 0.2\tau$. Each individual in the green zone can interact with a limited number (c_{visit}) of family members (hereafter “visitors”) from the orange zone per day. In some interventions we considered that individuals visiting the buffer zone will have a health check (e.g. temperature measurement), aimed at excluding symptomatic individuals. When the health check is applied, the transmission probability between individuals from the orange zone in the I or H compartments and individuals from the green zone is set to zero.

Although setting up a safety zone implies a reduction in the number of contacts between classes of the green zone and the orange zone, the mean number of contacts that each individual has per day, \bar{c}_i , is conserved. Therefore we need to estimate how contacts will be redistributed from individuals from a different zone to individuals living in the same zone. We model this redistribution of the contacts with the parameter ϵ_i :

$$\begin{aligned} \epsilon_i &= \rho c_{\text{visit}} / \bar{c}_i \quad (i, j \text{ in different zones}) \\ \epsilon_i &= 1 - \rho c_{\text{visit}} / \bar{c}_i \quad (i, j \text{ in same zone}). \end{aligned}$$

If we assume that visitors are always different, the quantity $f_{o,visit} = c_{visit} \frac{N_g}{N_o}$ is the fraction of the orange population that visits the buffer zone. We define ρ as¹:

$$\rho = \begin{cases} 1 & \text{if } i \in g \\ f_{o,visit} & \text{if } i \in o \end{cases}$$

Next, we model the probability of interaction between a member of class i and class j , depending on whether they belong to the same or to different zones. Since interaction is limited to others in the same zone, every individual will have a higher likelihood of interaction with members of the classes staying in the same zone compared to the null model. More specifically, the proportion N_i/N of individuals of class i in the null model will become N_i/N_X with N_X the total number of individuals in zone $X = \{o, g\}$. This yields the following values for m_{ij} :

$$\begin{aligned} m_{ij} &= \left(\frac{N_i}{N_X}\right) / \left(\frac{N_j}{N_X}\right) = \frac{N}{N_X} \quad (i, j \text{ in same zone } X) \\ m_{ij} &= \left(\frac{N_i}{N_Y}\right) / \left(\frac{N_j}{N_Y}\right) = \frac{N}{N_Y} \quad (i \in X \text{ and } j \in Y). \end{aligned}$$

We finally define the management matrix as $M_{ij} = \epsilon_i m_{ij}$.

Table 1: **Fraction of population in each zone by safety zone scenario and behaviour-class.** Behaviour-classes that are not considered in a given scenario have a proportion equal to zero.

Scenario	Age 1, orange	Age 1, green	Age 2 no comorbiditi- es, orange	Age 2 no comorbiditi- es, green	Age 2 comorbiditi- es, orange	Age 2 comorbiditi- es, green	Age 3 no comorbiditi- es, green	Age 3 comorbiditi- es, green
Only age 3 in green zone	.407	0	.471	0	.0626	0	.022	.0373
Age 3 + age 2 with comorbi- dities in green zone	.407	0	.471	0	0	.0626	.022	.0373
20% green zone capacity	.376	.0312	.424	.0469	0	.0626	.022	.0373
25% green zone capacity	.356	.0512	.394	.0769	0	.0626	.022	.0373
30% green zone capacity	.336	.0712	.364	.107	0	.0626	.022	.0373

Following this parameterization, we explore different scenarios, summarized in Table 1, for allocating members of each population class to the safety, or “green” zone, and the exposed, or “orange” zone. In one scenario, we only place individuals in age group 3 (>50) in the green zone, while in another we place all vulnerable individuals, age group 3 and age group 2 (13-50) with comorbidities, in the green zone. In 3 additional scenarios, after all

¹If c_{visit} is large enough ($c_{visit} \approx 15$ contacts per day), ρ should saturate, because every member of the orange zone would eventually visit the buffer zone, following the expression:

$$\rho = \begin{cases} 1 & \text{if } i \in g \\ f_{o,visit} \left(1 - H(f_{o,visit} - 1) \frac{f_{o,visit}-1}{f_{o,visit}}\right) & \text{if } i \in o \end{cases}$$

with the Heaviside function $H(f_{o,visit} - 1) = 1$ if $f_{o,visit} \geq 1$. We chose values well below this saturation threshold (a maximum of 10 contacts per week, i.e. 1.42 contacts per day).

vulnerable individuals are allocated to the green zone, we set the green zone's capacity to a certain percentage of the camp's population (20%, 25%, 30%), and allocate its remainder to non-vulnerable family members, who by necessity are either children <13 in age group 1 or healthy younger adults in age group 2. For these 3 scenarios, it is required to split the children and the healthy younger adults demographic-classes in two behaviour-classes (orange and green) to account for the different parameterizations in the contacts matrix, as explained above. In accordance with camp managers' expectations that many vulnerable individuals will have non-vulnerable spouses, while fewer vulnerable individuals will have young children, in these scenarios we allocate 40% of the remainder of the green zone to children and 60% of the remainder of the green zone to younger adults without comorbidities. We also consider a baseline scenario in which there is no green zone.

Estimation of the infectivity of the isolated and evacuated populations

To estimate the infectivity of the isolated population, we make the following assumptions. We considered a number N_{care} of carers having c_{care} contacts per day with the isolated population. Carers are entirely drawn from younger adults (age 2) with no comorbidities, and must have no symptoms. We denote the number of individuals fulfilling these requirements with N_{exp} (number of exposed). When the number of symptomatic individuals exceeds the isolation capacity, \tilde{N} , the individuals in excess are fully infectious (note that we use a tilde to denote variables related to the isolated population). In addition, the occupancy of the isolation beds is distributed among classes proportionally to the number of symptomatic individuals present in each class, i.e. $\tilde{I}_j = \tilde{N} (I_j / \sum_j I_j)$. Finally, symptomatic individuals developing symptoms that would require hospitalization, are either evacuated or become fully infectious. The rationale behind the latter choice is that camps lack the necessary means to adequately protect the rest of the population when individuals require more dedicated care. In particular, it is unlikely that a severely ill individual would be able to stay alone in a tent. We model evacuation considering a parameter $\epsilon = 0$ if evacuation is put in place and $\epsilon = 1$ otherwise. Evacuated individuals are no longer infectious.

Given these assumptions, to estimate the rate of exposure for each demographic-class, it is needed to split the contacts into two terms, one describing the interaction of individuals in the class with the isolated population, and another term for the infectious individuals that are not isolated:

$$\lambda_i = \tau \sum_j \underbrace{\beta_I \tilde{c}_i \tilde{P}(i \rightarrow j)}_{\text{isolated}} + C_{ij} \underbrace{\frac{\beta_P P + \beta_A A_j + \beta_I \Theta(N_I - \tilde{N})(I_j - \tilde{I}_j) + \epsilon \beta_H H_j}{N_j}}_{\text{not isolated}},$$

where \tilde{c}_i is the mean number of contacts of class i per individual per day with the self-isolated individuals and $\tilde{P}(i \rightarrow j)$ is the probability that an individual of class i encounters an isolated individual of class j . For the not-isolated term, we maintain the well-mixed population assumption explained in the Main Text, with the incorporation of a Heaviside function, $\Theta(N_I - \tilde{N})$, which activates the interaction with the clinical symptomatic individuals when their number N_I exceeds the isolation capacity \tilde{N} , and we estimate the probability of encountering with the non-isolated individuals to be proportional to their fraction $(I_j - \tilde{I}_j)/N_j$. For the isolated population, however, the well-mixed assumption is no longer valid. Firstly, all demographic-classes not contributing individuals to the group of carers will never interact with the isolated individuals, and hence $\tilde{c}_i = 0$ for them (morever $\tilde{P}(i \rightarrow j) = 0$). Secondly, the healthy younger adults population will certainly interact with isolated individuals due to their role of carers, hence $\tilde{P}(i \rightarrow j) = 1$.

To estimate \tilde{c}_i for the healthy younger adult class, we note that the number of contacts per day with the isolated individuals is $c_{\text{care}} N_{\text{care}}$, and hence the mean number of contacts per individuals per day is $\tilde{c}_i = c_{\text{care}} N_{\text{care}} / N_{\text{exp}}$. We observe that, increasing the number of carers, and the number of contacts per day between carers and individuals, will increase the rate of infection. For simplicity, we assume that there is one carer for each infected person in the class j , ($N_{\text{care},j} = \tilde{N}_j$), having only one contact per day (c_{care}). Note the convenience of this choice, since if the number of symptomatic individuals is larger than the number of potential carers, the ratio $\tilde{N}_j / N_{\text{exp}} > 1$, implying more than one contact per day is needed to take care of that population class.

We further assume that this interaction will be regulated through a buffer zone, so infectivity is reduced by 80%, denoted by $\xi = 0.2$.

With these considerations, the rate of infection for the healthy younger adult population class (indexed k) becomes:

$$\lambda_k = \tau \sum_j \xi \frac{\tilde{N}_j}{N_{\text{exp}}} + C_{kj} \frac{\beta_P P + \beta_A A_j + \beta_I \Theta(N_I - \tilde{N})(I_j - \tilde{I}_j) + \epsilon \beta_H H_j}{N_j},$$

For the remaining classes ($i \neq k$) the rate of infection becomes:

$$\lambda_i = \tau \sum_j C_{ij} \frac{\beta_P P + \beta_A A_j + \beta_I \Theta(N_I - \tilde{N})(I_j - \tilde{I}_j) + \epsilon \beta_H H_j}{\tilde{N}}.$$

A final consideration is that symptomatic individuals require some time to recognize their symptoms and to self-isolate. To model this, whenever simulating the isolation intervention, the symptomatic compartment is split in two compartments: onset of symptoms, I_i^{onset} , and symptomatic, I_i . We assumed the duration of I_i^{onset} follows a Gaussian distribution with means 12, 24 or 48 hours on average. The duration for which an individual isolates is then calculated as the difference between the symptomatic period if there is no isolation and the duration spent in the symptom onset compartment.

Supplementary figures

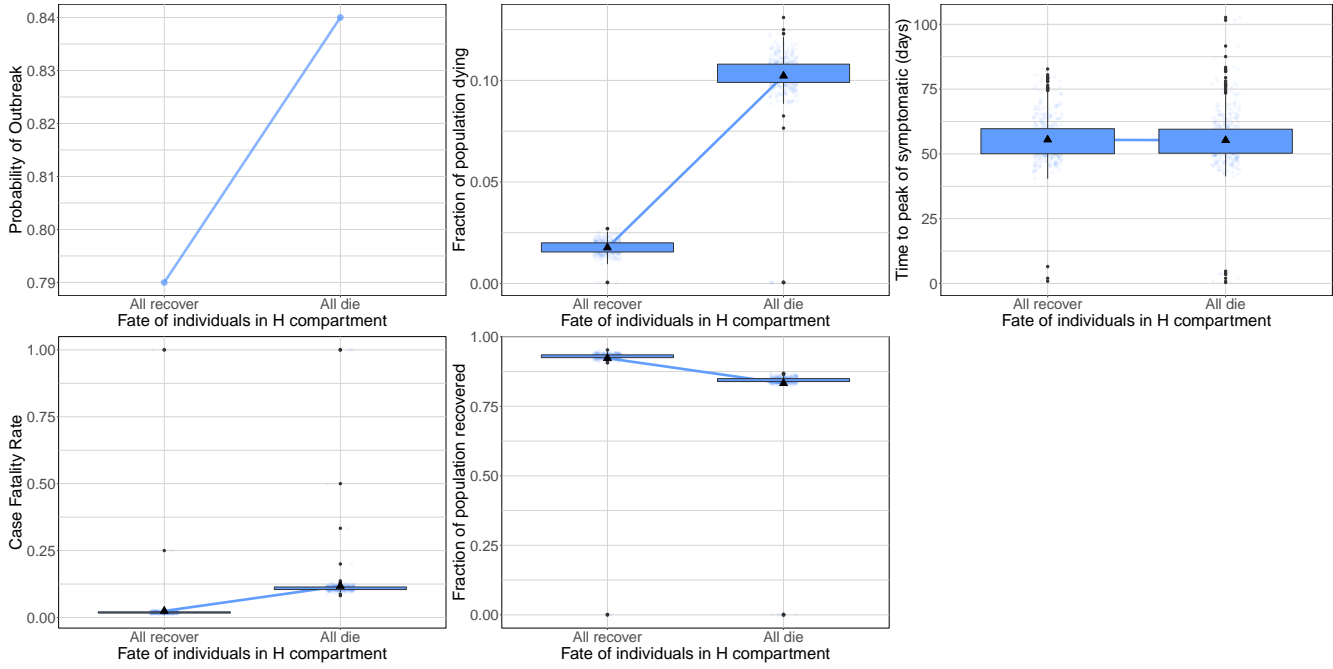


Figure 1: **Outcomes when all severe cases recover vs when all severe cases die.** Probability of an outbreak (top left), fraction of the population dying (top middle), time until peak symptomatic cases (top right), IFR (bottom left), and fraction of the population that recovers (bottom middle).

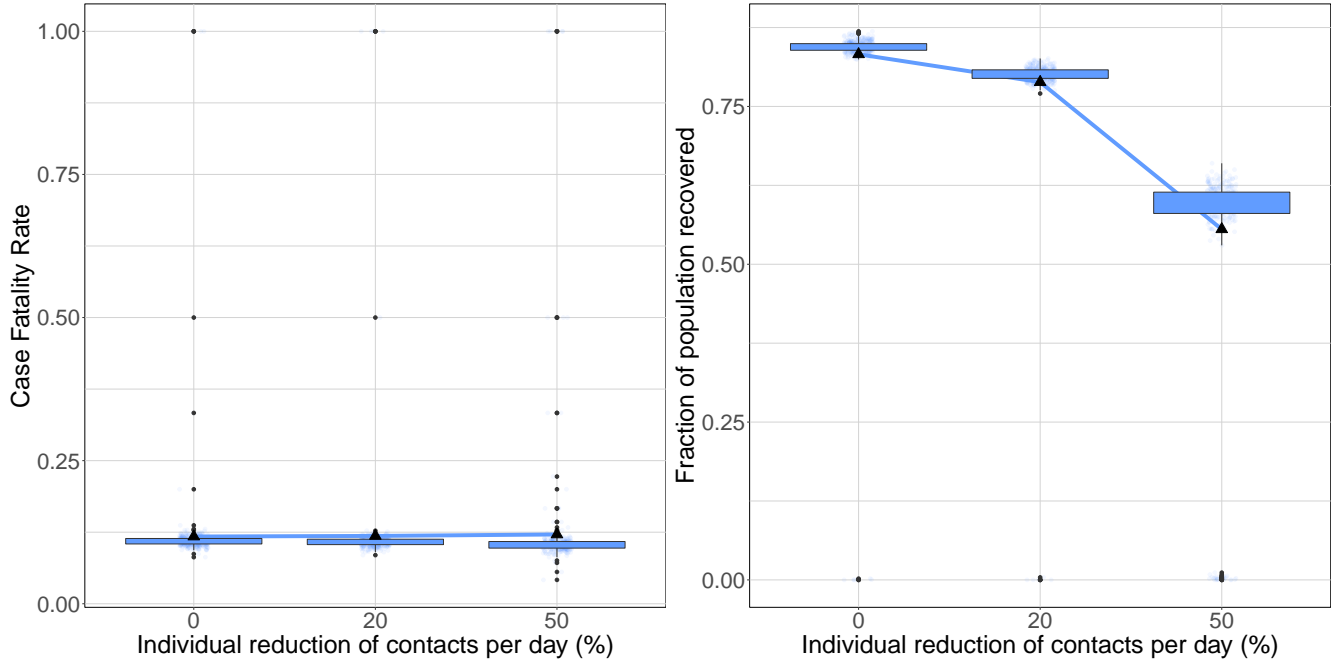


Figure 2: **Self-distancing.** IFR (left), and fraction of the population that recovers (right) as a function of the proportion of contacts reduced per individual per day.

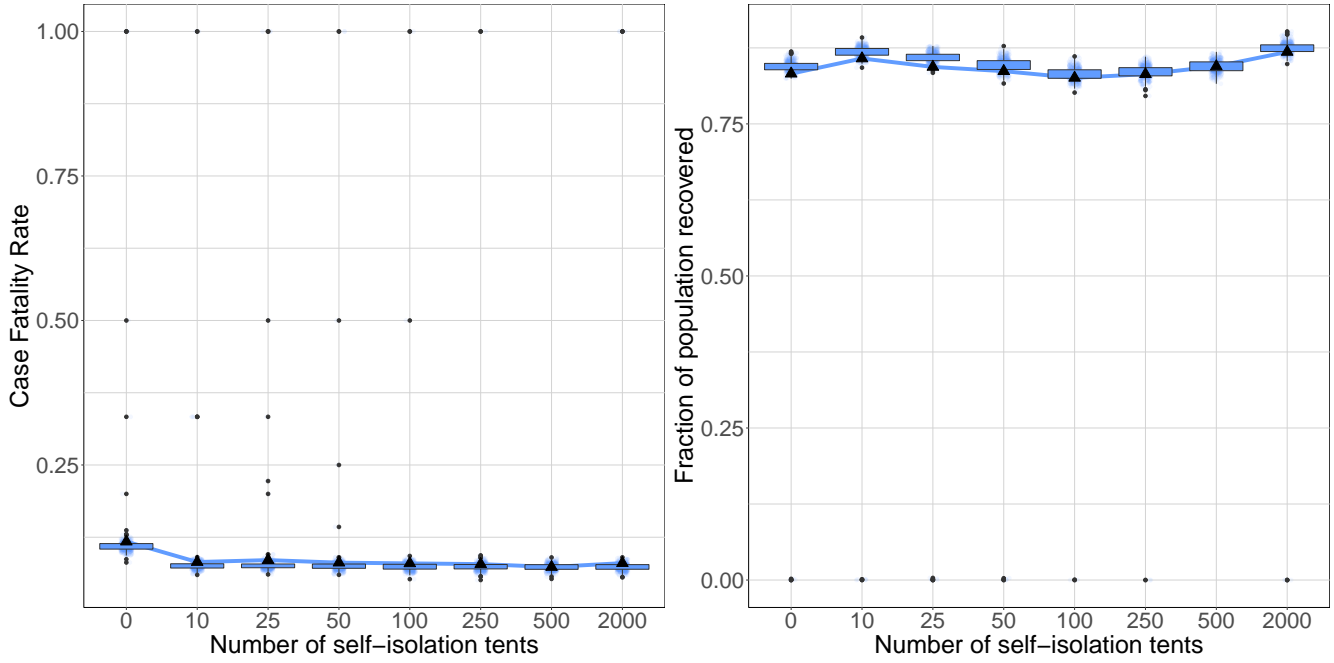


Figure 3: **Self-isolation.** IFR (left), and fraction of the population that recovers (right) as a function of the number of isolation tents available in the camp.

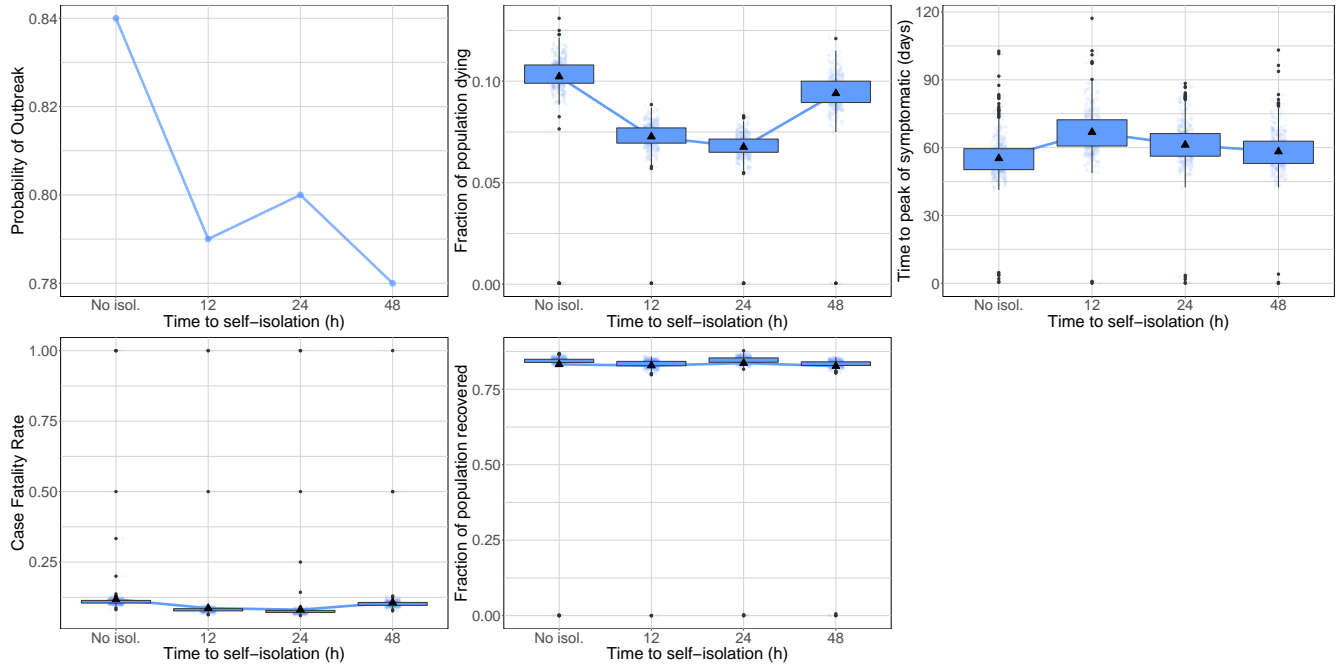


Figure 4: **Time to self-isolation.** Probability of an outbreak (top left), fraction of the population dying (top middle), time until peak symptomatic cases (top right), IFR (bottom left), and fraction of the population that recovers (bottom middle) as a function of the time that individuals require to recognize their symptoms and self-isolate.

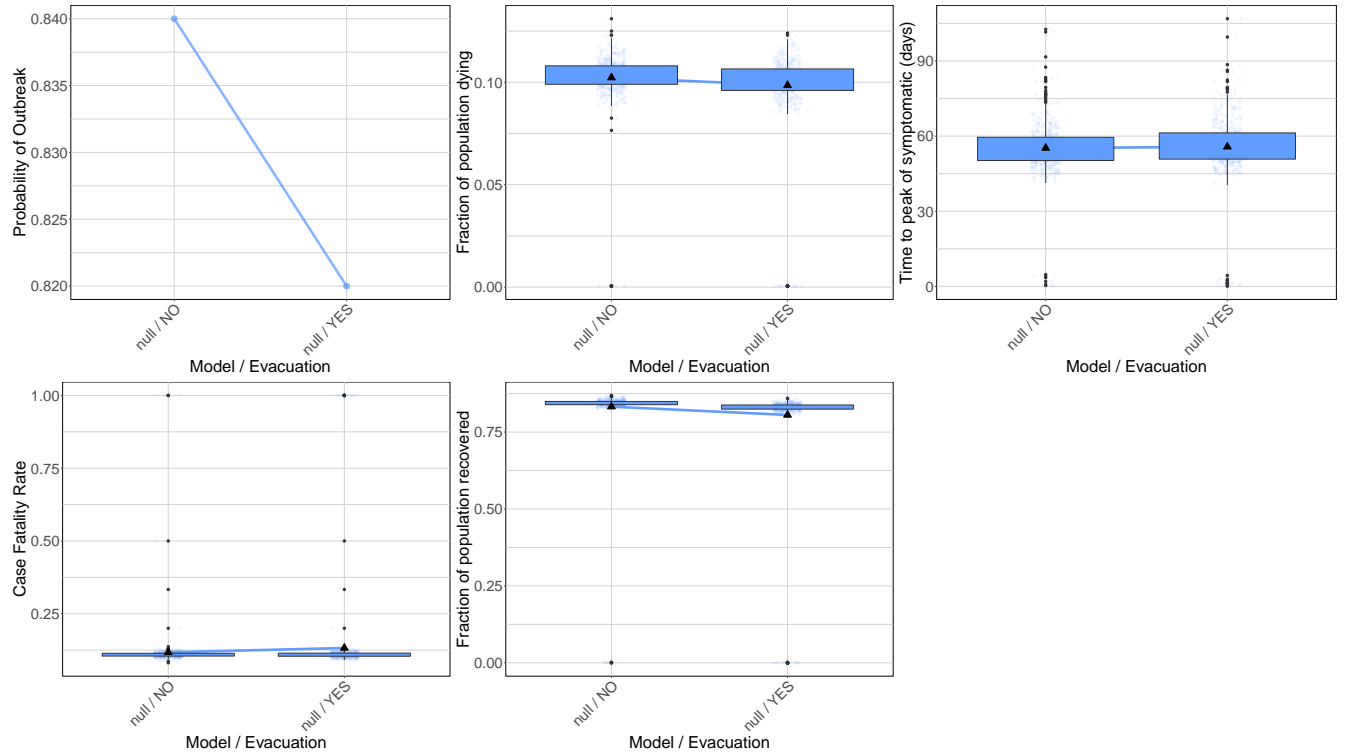


Figure 5: **Evacuation.** Probability of an outbreak (top left), fraction of the population dying (top middle), time until peak symptomatic cases (top right), IFR (bottom left), and fraction of the population that recovers (bottom middle), as a function of whether individuals requiring hospitalization are evacuated to isolation centers.

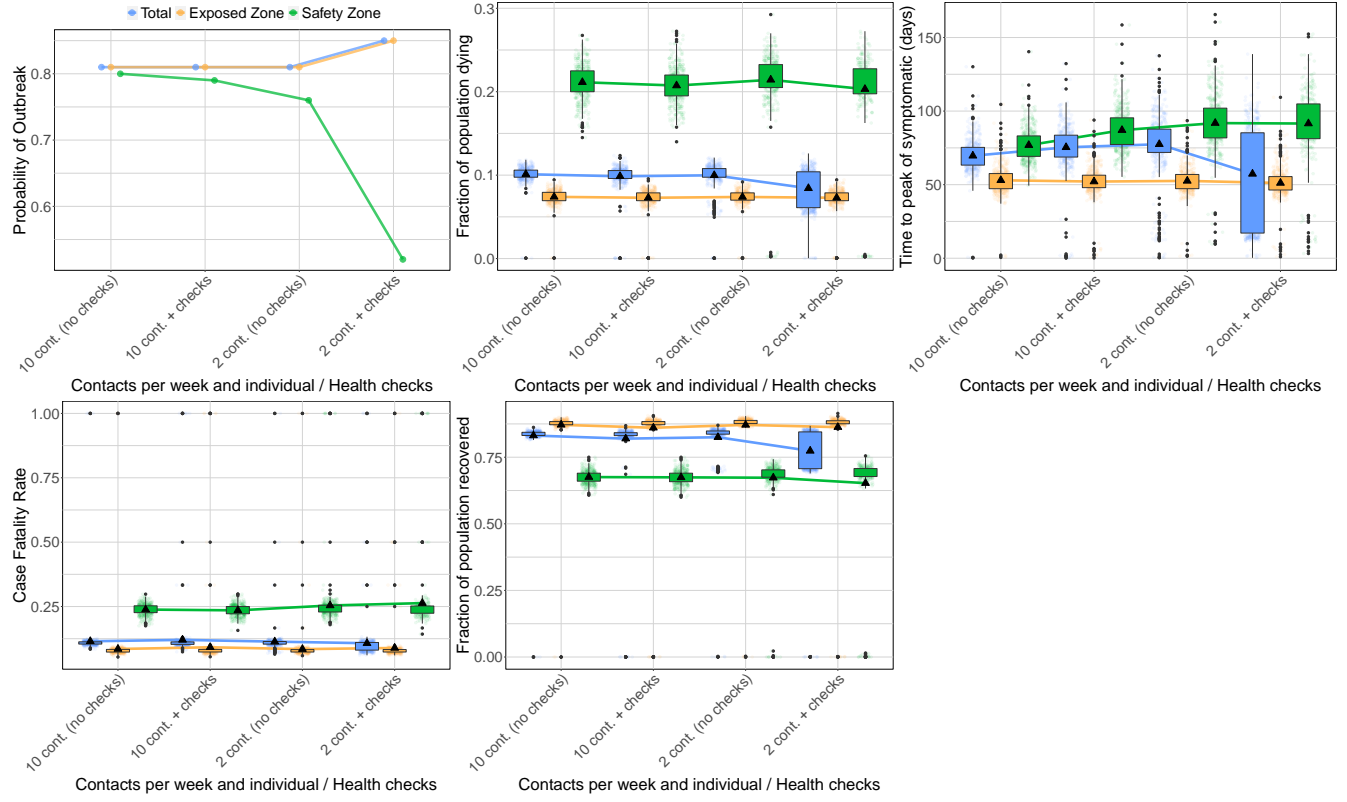


Figure 6: Health-checks in the buffer zone. Probability of an outbreak (top left), fraction of the population dying (top middle), time until peak symptomatic cases (top right), IFR (bottom left), and fraction of the population that recovers (bottom middle), as a function of whether health-checks are implemented in the buffer zone between the safety and exposed zones. Scenarios with 10 or 2 contacts in the buffer zone per person in the safety zone per week are plotted. All figures consider the scenario in which 20% of the camp's population is allocated to the safety zone.

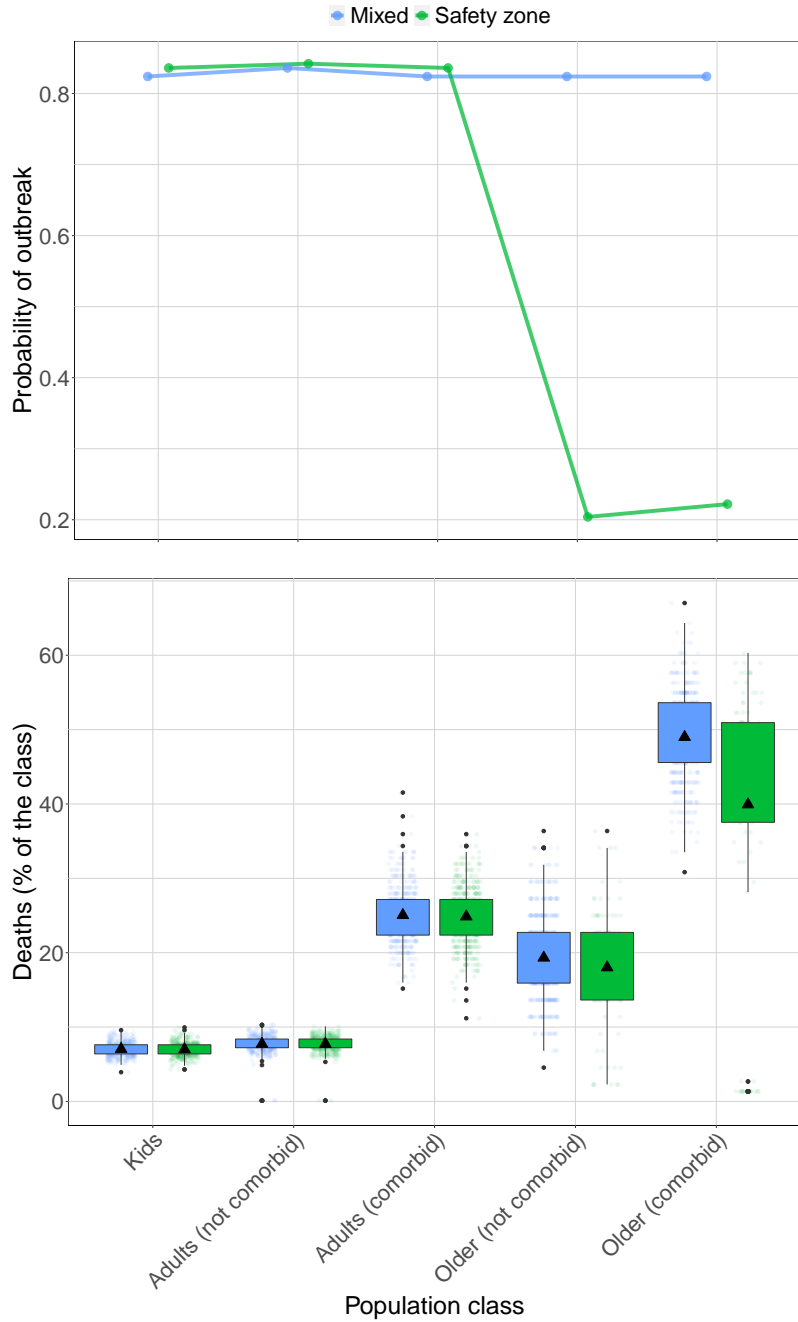


Figure 7: Effects of the safety zone on outcomes by population class. Probability of an outbreak (top), and proportion that dies in each population class (bottom) when no interventions are implemented (Mixed), compared to protection of older adults in the safety zone with 2 contacts in the buffer zone per week (Safety zone). The fraction of deaths in the safety zone for the older population is significantly lower (Kruskal-Wallis test, $p\text{-val} < 10^{-15}$).

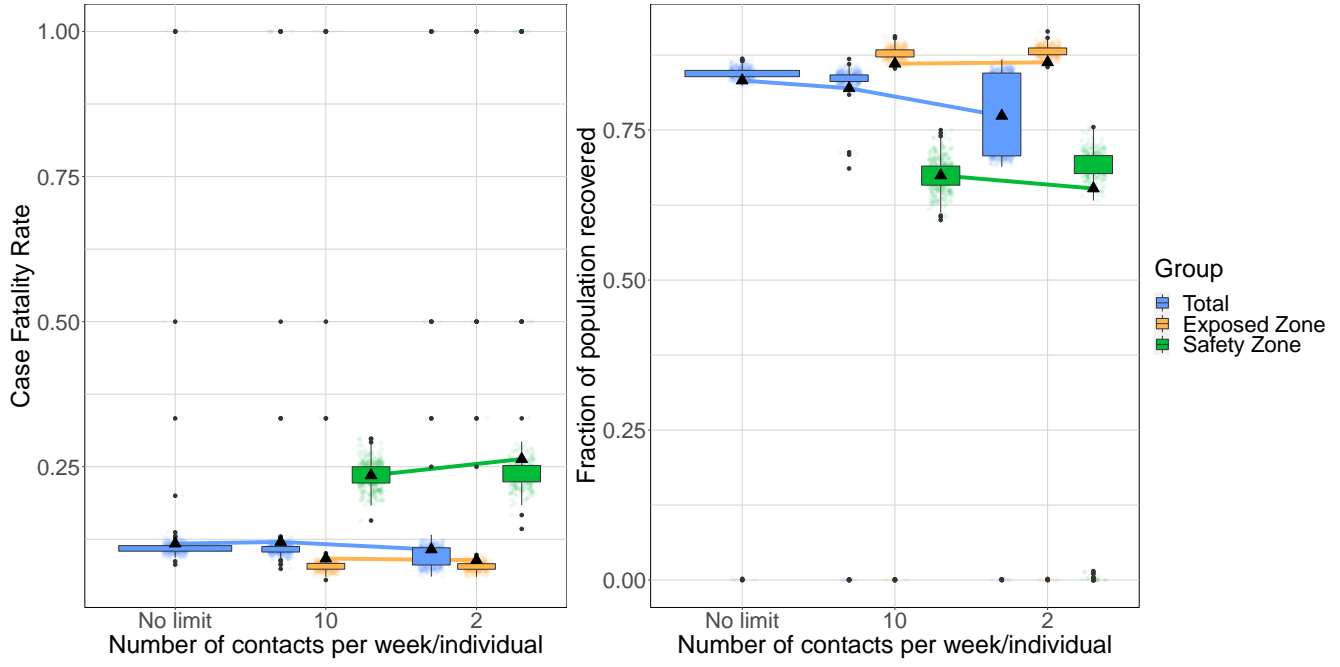


Figure 8: **Number of contacts in the buffer zone.** IFR (left), and fraction of the population that recovers (right) as a function of the number of contacts that each individual in the safety zone has in the buffer zone per week. All figures consider the scenario in which 20% of the camp's population is allocated to the safety zone.

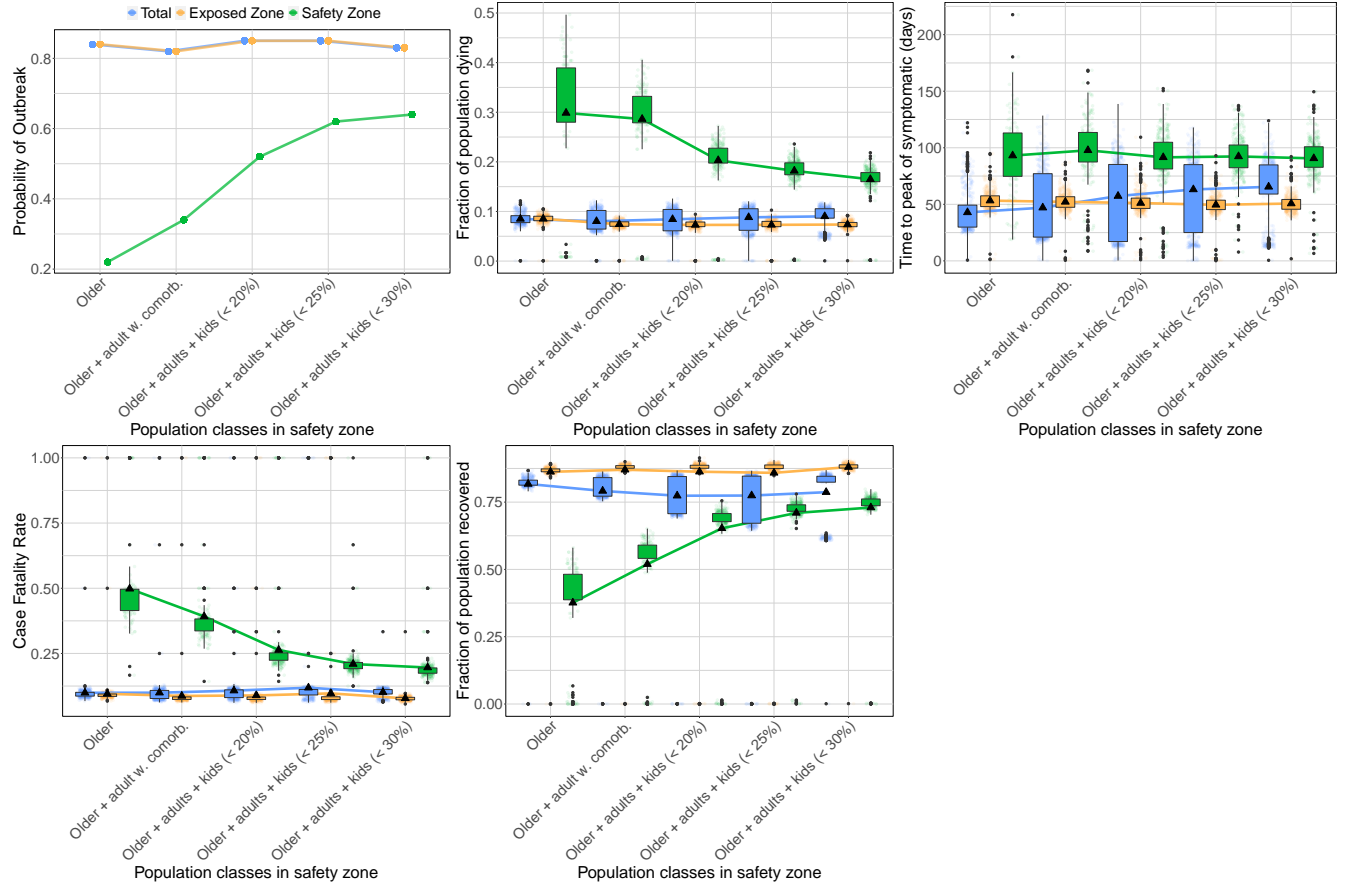


Figure 9: Population moving to the safety zone. Probability of an outbreak (top left), fraction of the population dying (top middle), time until peak symptomatic cases (top right), IFR (bottom left), and fraction of the population that recovers (bottom middle) as a function of the safety zone allocation scenario (see Table 1). All figures consider the scenario with 2 contacts in the buffer per person in the safety zone per week.

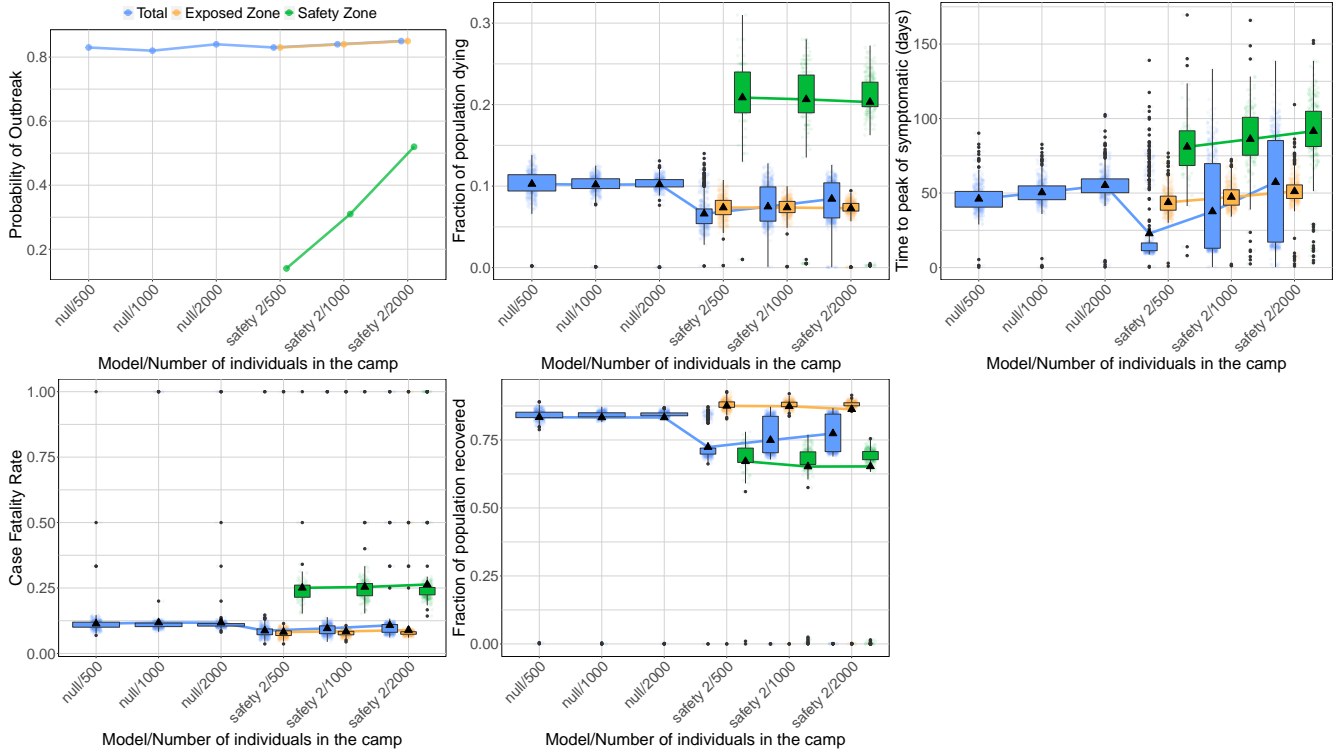


Figure 10: **Efficacy of the safety zone for different population sizes.** Probability of an outbreak (top left), fraction of the population dying (top middle), time until peak symptomatic cases (top right), IFR (bottom left), and fraction of the population that recovers (bottom middle) as a function of the total population size. The figures consider scenarios with no interventions (null), and with a safety zone comprising 20% of the camp's population with 2 contacts in the buffer zone per person in the safety zone per week (safety 2).

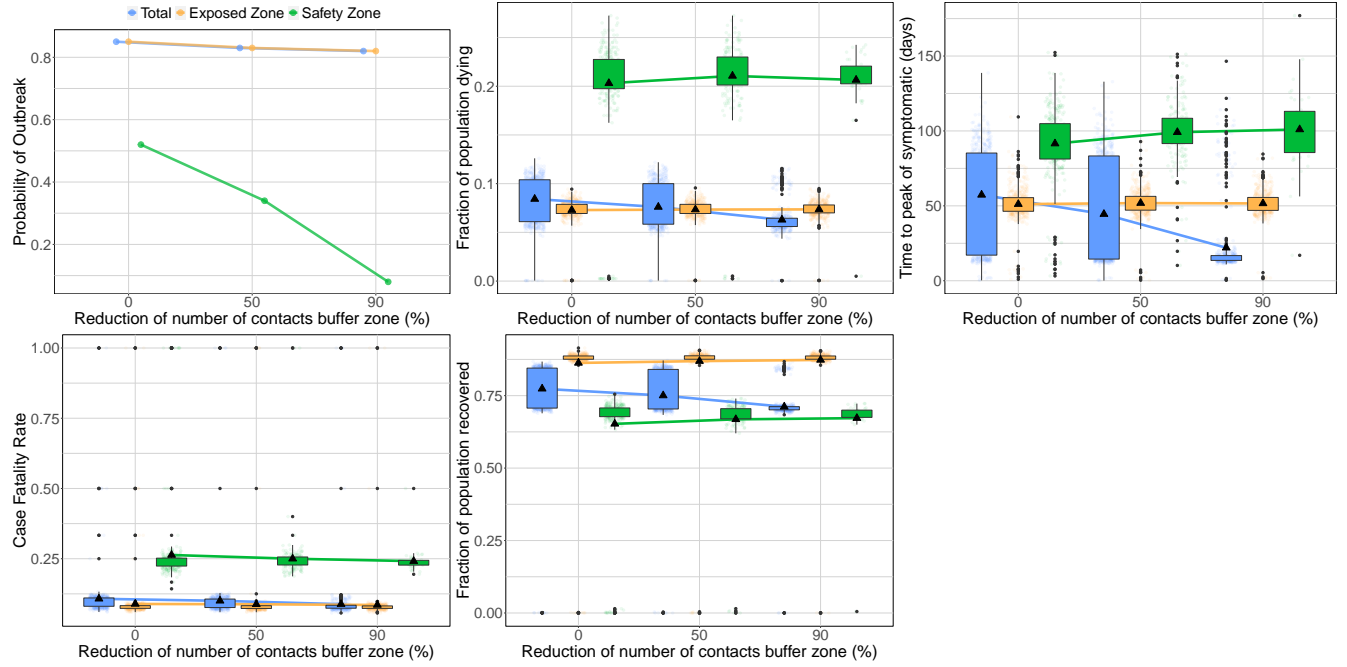


Figure 11: **Lockdown of the safety zone.** Probability of an outbreak (top left), fraction of the population dying (top middle), time until peak symptomatic cases (top right), IFR (bottom left), and fraction of the population that recovers (bottom middle) as a function of the reduction in the number of contacts permitted in the buffer zone from a baseline of 2 per person in the safety zone per week. All figures consider the scenario in which 20% of the camp's population is allocated to the safety zone.

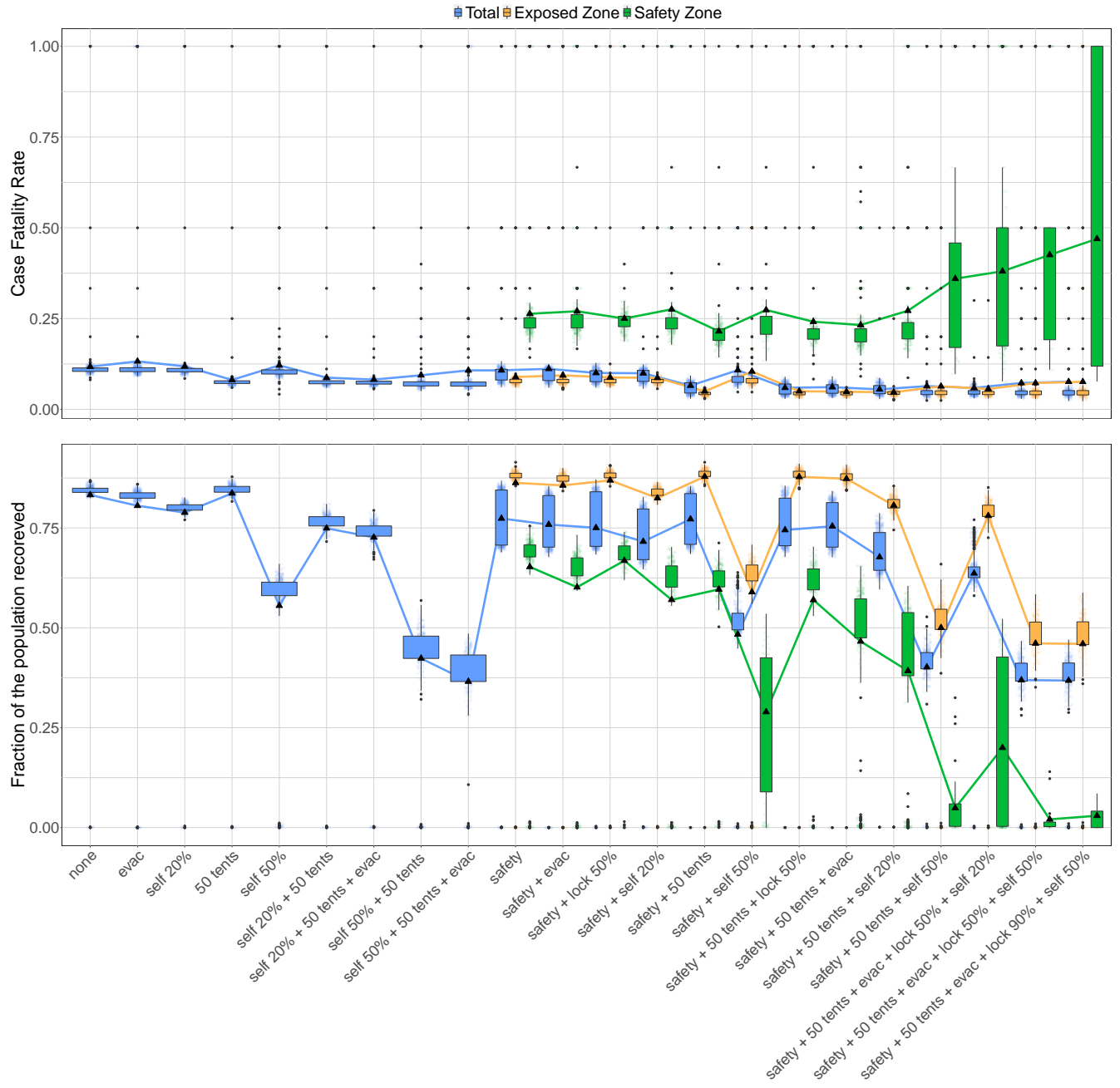


Figure 12: **Combined interventions.** IFR (top), and fraction of the population that recovers (bottom) for different combinations of interventions. Evac = evacuation of severely symptomatic, self = self-distancing, tents = number of available self-isolation tents, safety = safety zone, lock = lockdown of the buffer zone. For combinations of interventions including a safety zone, we distinguish between the population living in the green zone, in the orange zone and the whole population. The increase in the IFR for the green zone is explained by the discretization of the possible values that the IFR can take when the number of cases is very low (see Supplementary Table 2).

Intervention	<20 cases	Total	% of total
safety	16	270	5.9
safety + evac	20	249	8
safety + lock 50%	5	171	2.9
safety + self 20%	19	188	10
safety + 50 tents	11	240	4.6
safety + self 50%	14	64	22
safety + 50 tents + lock 50%	14	154	9.1
safety + 50 tents + evac	33	239	14
safety + 50 tents + self 20%	31	144	22
safety + 50 tents + self 50%	25	38	66
safety + 50 tents + evac + lock 50% + self 20%	53	110	48
safety + 50 tents + evac + lock 50% + self 50%	18	20	90
safety + 50 tents + evac + lock 90% + self 50%	6	8	75

Table 2: **Efficacy of the safety zone in combination with other interventions.** <20 cases = number of outbreaks in the green zone with fewer than 20 cases recorded. Total = total number of simulations where an outbreak in the green zone occurs (at least one death). % of total = percent of outbreaks where fewer than 20 cases are recorded. N = 500 simulations for each combination of interventions. For the most effective combinations, the majority of simulations where an outbreak occurs in the green zone see fewer than 20 cases. In these simulations, the discretization of the possible values that the IFR can take explains its apparently anomalous increase in Fig. 12.

References

- [1] Xi He, Eric HY Lau, Peng Wu, Xilong Deng, Jian Wang, Xinxin Hao, Yiu Chung Lau, Jessica Y Wong, Yujujuan Guan, Xinghua Tan, et al. Temporal dynamics in viral shedding and transmissibility of covid-19. *Nature medicine*, 26(5):672–675, 2020.
- [2] Peter Ashcroft, Jana S. Huisman, Sonja Lehtinen, Judith A. Bouman, Christian L. Althaus, Roland R. Regoes, and Sebastian Bonhoeffer. COVID-19 infectivity profile correction. *arXiv:2007.06602 [q-bio, stat]*, July 2020. arXiv: 2007.06602.
- [3] Jennifer Harcourt, Azaibi Tamin, Xiaoyan Lu, Shifaq Kamili, Senthil K Sakthivel, Janna Murray, Krista Queen, Ying Tao, Clinton R Paden, Jing Zhang, et al. Severe acute respiratory syndrome coronavirus 2 from patient with coronavirus disease, united states. *Emerging infectious diseases*, 26(6):1266, 2020.
- [4] Dawei Wang, Bo Hu, Chang Hu, Fangfang Zhu, Xing Liu, Jing Zhang, Binbin Wang, Hui Xiang, Zhenshun Cheng, Yong Xiong, et al. Clinical characteristics of 138 hospitalized patients with 2019 novel coronavirus-infected pneumonia in wuhan, china. *Jama*, 323(11):1061–1069, 2020.
- [5] Jeroen J.A. van Kampen, David A.M.C. van de Vijver, Pieter L.A. Fraaij, Bart L. Haagmans, Mart M. Lamers, Nisreen Okba, Johannes P.C. van den Akker, Henrik Endeman, Diederik A.M.P.J. Gommers, Jan J. Cornelissen, Rogier A.S. Hoek, Menno M. van der Eerden, Dennis A. Hesselink, Herold J. Metselaar, Annelies Verbon, Jurriaan E.M. de Steenwinkel, Georgina I. Aron, Eric C.M. van Gorp, Sander van Boheemen, Jolanda C. Voermans, Charles A.B. Boucher, Richard Molenkamp, Marion P.G. Koopmans, Corine Geurtsvankessel, and Annemiek A. van der Eijk. Shedding of infectious virus in hospitalized patients with coronavirus disease-2019 (COVID-19): duration and key determinants. *medRxiv*, page 2020.06.08.20125310, January 2020.
- [6] Assistance Coordinator Unit. The Syrian IDP camps monitoring study - Northern Syria camps - Humanitarian Data Exchange. url: <https://data.humdata.org/dataset/idp-camps-monitoring-november-of-2018>.
- [7] HelpAge International and Handicap International. Hidden victims of the Syrian crisis: disabled, injured and older refugees. Technical report, HelpAge International and Handicap International, April 2014. type: dataset.
- [8] Yuanyuan Dong, Xi Mo, Yabin Hu, Xin Qi, Fang Jiang, Zhongyi Jiang, and Shilu Tong. Epidemiological characteristics of 2143 pediatric patients with 2019 coronavirus disease in china. *Pediatrics*, 2020.
- [9] Nancy Chow, Katherine Fleming-Dutra, Ryan Gierke, Aron Hall, Michelle Hughes, Tamara Pilishvili, Matthew Ritchey, et al. Preliminary estimates of the prevalence of selected underlying health conditions among patients with coronavirus disease 2019 in usa, february 12–march 28, 2020. *Morbidity and Mortality Weekly Report*, 69(13):382, 2020.
- [10] O. Diekmann, Hans Heesterbeek, and Tom Britton. *Mathematical tools for understanding infectious diseases dynamics*. Princeton series in theoretical and computational biology. Princeton University Press, Princeton, 2013.
- [11] Sydney Philipps, Dan Rossi, Rachel Von Arb, and Alex Capaldi. Mathematical models of infectious diseases: Two-strain infections in metapopulations, July 2011.
- [12] Marino Gatto, Enrico Bertuzzo, Lorenzo Mari, Stefano Miccoli, Luca Carraro, Renato Casagrandi, and Andrea Rinaldo. Spread and dynamics of the COVID-19 epidemic in Italy: Effects of emergency containment measures. *Proceedings of the National Academy of Sciences*, 117(19):10484–10491, May 2020.
- [13] J.M Heffernan, R.J Smith, and L.M Wahl. Perspectives on the basic reproductive ratio. *Journal of the Royal Society Interface*, 2(4):281–293, sep 2005.